Hierarchical structuring of cathodes and anodes for lithium-ion batteries

N. Straßburger*, P. Zhu, W. Pfleging
Karlsruhe Institute of Technology, Institute for Applied Materials – Applied Materials Physics,
Hermann-von-Helmholtz-Platz 1, 76344 Eggenstein-Leopoldshafen, Germany

ABSTRACT

Extensive technological progress is essential to meet the ambitious future requirements of energy storage devices. This is due to the necessity of achieving high energy and power density operations, accompanied by high safety standards and extended lifespans, while maintaining low production and material costs. Significant importance is placed on the research of high energy active materials. However, besides material optimization, there is substantial potential for optimization by introducing electrodes with high mass loading, advanced electrode architectures, and their transfer to production level. Achieving appropriate trade-offs between high energy and power density, process reliability, and economic considerations poses a challenge for current lithium-ion battery technology.

For this purpose, the laser-assisted generation of three-dimensional (3D) electrode architectures is studied and evaluated. Advanced electrode design incorporates micro and sub-micron structures that can be designed in various ways. Significant improvements in battery lifespan and high-power operation capabilities can be achieved compared to traditional two-dimensional (2D) electrodes.

Furthermore, the production of 3D electrodes with laser processing requires coordination with other established manufacturing steps in the battery production process. In particular, the calendering of electrodes holds great importance as it has a significant impact on the microstructural properties of the composite electrode, including porosity, material density, and film adhesion strength. This study investigated the impact of laser-induced hierarchical structuring, comprising micro-/nano-porosities and microtopography, on electrodes with varying mass loadings from 2 mAh/cm² to 6 mAh/cm². In this regard, cells comprising graphite anodes and lithium-nickel-manganese-cobalt oxide cathodes were prepared and subjected to electrochemical characterization techniques.

Keywords: 3D battery, ultrafast laser structuring, calendering, lithium nickel manganese cobalt oxide, graphite

1. INTRODUCTION

Meeting the evolving demands of energy storage solutions requires significant advancements in technology. This necessity is based on the goal of achieving high energy and power density, enhanced safety standards, and prolonged device lifespans, all while keeping production and material costs low. In this field, lithium-ion battery (LIB) technology stands as the dominant energy storage solution and is anticipated to maintain this distinction for the forthcoming decade, particularly within the transportation sector. This is because LIBs offer advantageous features such as their relatively high energy and power densities. In order to enhance this technology, there is a focused effort on the exploration of high-energy active materials.[1]

The deployment of active materials with high specific capacity and the utilization of thick-film electrodes, which reach thicknesses of 100 µm and beyond, contribute to the high energy densities of up to 550 $Wh \cdot l^{-1}$ that are seen in today's commercial LIBs. This helps to extend driving ranges of battery electric vehicles (BEVs) up to 500 km, a comparable distance to vehicles powered by internal combustion engines.[2-4]

Beyond material advancements, there are significant opportunities for optimization by incorporating electrodes with increased mass loading, innovative electrode designs, and transitioning these advancements to production scales. However, striking the right balance between high energy and power density, manufacturing reliability, and cost-effectiveness remains a challenge for current LIB technologies. To address these challenges, there is a possibility to improve the aforementioned aspects with a laser-assisted generation of three-dimensional (3D) structures in electrodes. This method, which is currently being evaluated, presents promising opportunities for improving LIB. This advanced

battery design allows for the incorporation of micro and sub-micron features in diverse configurations. Such designs with for example line, grid or hole structures have demonstrated substantial benefits in reduced mechanical degradation, better electrolyte wetting, improved high-rate capability and lower risk of lithium plating compared to traditional two-dimensional (2D) designs. For the fabrication of 3D electrodes high-power ultrafast laser ablation has proven to be effective. However, laser ablation process must be harmonized with other established production steps in battery manufacturing.[5-9]

The calendering process of electrodes, in particular, is crucial as it significantly affects the microstructural characteristics of the electrode material, such as porosity, electronic conductivity, density, wettability, and layer cohesion. Investigations have explored the effects which includes micro-/nano-porosities and microtopography on the electrodes with different mass loadings, while the resulting electrochemical properties were thoroughly assessed.[10-12]

In this study, we focus on exploring the potential of laser-assisted 3D electrode structures to address the challenges faced by current LIB technologies. Specifically, we investigate the effects of laser-induced hierarchical structuring on electrodes with varying mass loadings and porosities, employing graphite anodes and lithium-nickel-manganese-cobalt oxide (NMC) cathodes. Through comprehensive electrochemical characterization techniques, we aim to shed light on the impact of these advanced electrode designs on battery performance.

2. EXPERIMENTAL

2.1 Electrode manufacturing

To fabricate the cathodes, NMC 622 (BASF, Germany) was mixed with conductive graphite and carbon black (C-nergy Super C65, Imerys G&C, Switzerland) using a polyvinylidene fluoride (PVDF, Solef® 5130, Solvay Specialty Polymers, France) binder dissolved in N-methyl-2-pyrrolidone (NMP, Merck KGaA, Germany), as detailed in Table 1. The binder solution was blended at a weight ratio of 1:10 (PVDF : NMP) in a centrifugal mixer (SpeedMixer DAC 150 SP, Hauschild & Co., Germany). The cathode slurry was homogenized using the same mixer with rotating speeds varying from 1000 to 3500 rpm for about 2 hours, and was then coated onto aluminum foil with a thickness of 20 µm using a doctor blade and subsequently dried at 90°C for 2 hours. The cathodes were designed with areal capacities of 2, 4, and 6 mAh/cm², corresponding to varying thicknesses of the electrodes.

Table 1: Material and mass fraction of the NMC 622 slurry.

Material	Mass fraction [wt.%]
NMC 622	92
Carbon black (SC65)	3
Conductive graphite (KS6L)	3
PVDF binder	2
NMP solvent	-

As for the preparation of anode, sodium carboxymethyl cellulose (CMC, MTI Corporation, USA) was mixed in water using a lab dissolver (DB13, DISTECH GmbH, Germany) to obtain a 1.3 wt.% solution. Afterwards, graphite (SPGPT808, Targray Inc., Canada) and carbon black (Timcal Super C65, MTI Corporation, USA) were added into the solution and mixed at 2500 rpm for 90 min. Styrene-butadiene rubber (SBR) solution (50 wt.% solid content, MTI Corporation, USA) was then added into the homogenized mixture and was further mixed at a low speed of 500 rpm. The mass fraction of each component in anode slurry is detailed in Table 2. The resultant anode slurry was coated onto a 10 µm thick copper foil using the doctor blade and dried for 1 hour at 85°C prior to calendering. The negative/positive ratio (N/P) of the cell components was maintained between 1.15 and 1.3.

Table 2: Material and mass fraction of the graphite slurry.

Material	Mass fraction [wt.%]
SPGPT808	93.00
Carbon black (SC65)	1.40
1.3 wt.% CMC solution	1.87
SBR solution	3.73

After drying, the electrodes were cut into sheets measuring 200 x 240 mm² for the cathodes and 200 x 200 mm² for the anodes. Calendering was executed on a rolling press (MX1009010, Saueressig GmbH & Co. KG, Germany) with a constant roller temperature of 50 °C. Due to the notable "spring back" effect observed in the calendered films, a subsequent calendering step was conducted using a second rolling press (HR01, MTI Corporation, USA) to achieve the desired porosity values. The porosity values were selected to ensure that on the one hand, the coating has sufficient adhesive strength; and on the other hand, no crack formation should take place in calendered electrodes. This guarantees no negative influence of the calendering process on the subsequent laser process. The porosities for cathodes and anodes were adjusted to 34 – 45% and 22 – 35%, respectively.

2.2 Electrochemical analyses

The coin cell CR2032 design was used for the electrochemical analyses. Anodes and cathodes were laser cut in diameter of 15 mm and 12 mm, respectively, and dried for 16 hours at 130°C in a vacuum oven. These components were then assembled in coin cells within an argon-filled glove box (LAB master pro sp, M. Braun Intergas-Systeme GmbH, Garching, Germany). Each cell consisted of an anode, a cathode, 120 µl of electrolyte (1 M $LiPF_6$ in a mixture of ethylene carbonate and ethyl methyl carbonate at a 3:7 volumetric ratio, with 2 wt.% vinylene carbonate additive), and a 25 µm polypropylene separator (Celgard LLC., USA), two 500 µm spacers and a wave spring. After assembly, all cells were stored at 20 °C for 24 hours to ensure complete saturation of the components with the electrolyte before starting the electrochemical analysis.

The formation of the cells involved two cycles: charging under constant current (CC), transitioning to constant voltage (CV), and then discharging under CC at a C/20 rate, with a cut-off current set at C/40. A voltage window of 2.8 V to 4.2 V was applied for all cells. Following this, the cells with the reference cathodes (35% porosity) and anodes with varying porosities were subjected to a asymmetric charging protocol as detailed in Table 3, while the cells with the reference anodes (40% porosity) and cathodes with varying porosities were subjected to a asymmetric discharging protocol as listed in Table 4. A 15-minute rest period was incorporated between each charging and discharging phase, while a four-hour rest period was set after the last cycle at each C-rate in order to examine the voltage stability after rapid charging. Additionally, for the fifth cycle of each C-rate assessment, the CV phase was limited to 15 minutes, aligning with the current limitations specified in Table 3 and Table 4. The determination of the C-rate was based on the discharge capacity recorded from the second formation cycle. The C-rate describes how quickly a battery is charged or discharged, where for example 1C stands for charging or discharging in one hour and C/2 for charging or discharging in two hours.

Table 3: Protocol applied for the rate capability analyses with asymmetric charging.

Charging protocol							
Charging CC	0.1C	0.2C	0.5C	1C	2C	3C	5C
Charging CV	0.05C	0.1C	0.1C	0.1C	0.1C	0.1C	0.1C
Discharge CC	0.1C	0.2C	0.2C	0.2C	0.2C	0.2C	0.2C
Repetitions	5C	5C	5C	5C	5C	5C	5C

Table 4: Protocol applied for the rate capability analyses with asymmetric discharging.

Discharging protocol							
Charging CC	0.1C	0.2C	0.2C	0.2C	0.2C	0.2C	0.2C
Charging CV	0.05C	0.1C	0.1C	0.1C	0.1C	0.1C	0.1C
Discharge CC	0.1C	0.2C	0.5C	1C	2C	3C	5C
Repetitions	5C	5C	5C	5C	5C	5C	5C

2.3 Laser structuring

One aim of this study was to explore the ablation behavior of both weakly and strongly calendered NMC 622 cathodes and graphite anodes. To maintain consistency in the study, a fixed pulse spacing of 13.3 µm and a pulse energy of 26.6 µJ were applied across the experimental setups 1 to 4. The first three experimental setups employed a high-repetition-rate laser source (Tangerine, Amplitude Laser, France) within a laser micromachining system (PS450-TO, Optec s.a., Belgium). In setups 1 and 2, the laser was operated at a wavelength of 1030 nm, while a wavelength of 515 nm was applied in setup 3, with an average maximum laser power of 34.3W at 1030 nm and 14.6 W at 515 nm, at a repetition rate of 200 kHz. In setup 1, the pulse duration was set to 440 fs, in setup 2 to 10 ps, and in setup 3 to 360 fs. Line patterns with a spacing of 200 µm were created using an average laser power of 8 W, a repetition rate of 300 kHz, and a scanning speed of 4 m/s. In setups 1 and 2, the number of passes was set consistently to 68, while in setup 3 the number of passes was set to 38.

In the second phase of the study, electrodes with the lowest and highest layer thicknesses were selected. The fourth setup involved a high-power laser source (FX600-2-GFH, EdgeWave GmbH, Germany) in another laser micromachining system (MSV203 Laser Patterning Tool, M-SOLV LTD, UK). This laser, operating at a wavelength of 1030 nm, reached a maximum average power of 300 W, a pulse length of 600 fs, and an optimized repetition rate of 1.5 MHz. Here, line patterns were structured with an average laser power of 40 W, a repetition rate of 1.5 MHz, a scanning speed of 20 m/s, and a variable number of passes to expose the current collector. The pitch remained at 200 µm.

3. RESULTS AND DISCUSSION

3.1 Electrode manufacturing

The following Table 5 and Table 6 present detailed parameters related to the film thickness, achieved porosity, and areal capacity of both NMC 622 cathodes and graphite anodes used in the study. For each type of electrode, the table delineates the variations in film thickness and correlates these measurements with the respective porosities achieved through the calendering process and the respective areal capacity.

Table 5: Film thickness, achieved porosity, and areal capacity of the NMC 622 cathodes.

Calendered film thickness [µm]	Achieved porosity [%]	Areal capacity [mAh/cm2]
35 ± 0.7	21.7	1.87 ± 0.02
41 ± 0.5	30.1	1.94 ± 0.01
44 ± 0.6	34.4	1.88 ± 0.03
76 ± 1.2	23.8	3.79 ± 0.02
78 ± 0.8	29.1	3.55 ± 0.01
88 ± 0.5	33.8	3.73 ± 0.03
111 ± 0.6	23.2	5.44 ± 0.01
119 ± 1.1	28.6	5.46 ± 0.01
131 ± 0.5	34.0	5.63 ± 0.04

Table 6: Film thickness, achieved porosity, and areal capacity of the graphite anodes.

Calendered film thickness [µm]	Achieved porosity [%]	Average areal capacity [mAh/cm^2]
55 ± 0.9	34.5	2.30 ± 0.00
59 ± 0.5	39.2	2.32 ± 0.02
63 ± 0.4	43.0	2.33 ± 0.00
106 ± 1.2	34.5	4.40 ± 0.01
116 ± 1.1	40.1	4.37 ± 0.04
125 ± 1.1	44.2	4.38 ± 0.01
158 ± 1.1	34.0	6.64 ± 0.00
175 ± 1.1	40.5	6.66 ± 0.02
186 ± 0.5	43.9	6.60 ± 0.00

3.2 Electrochemical analyses

An analysis of the electrochemical properties of cells made of electrodes with different porosities was conducted by an asymmetric charging rate test and an asymmetric discharging rate test. The specific charge capacities in Figure 1a and discharge capacities in Figure 1b of the NMC 622 as a function of the applied C-rate are shown in Figure 1.

For both types of configuration, whether it be the high porosity anode (44 % porosity) depicted in blue versus the low porosity anode (34 % porosity) in red shown in Figure 1a, or the high porosity cathode (35 % porosity) in blue versus the low porosity cathode (30 % porosity) in red shown in Figure 1b, the same pattern can be observed: cells containing the higher porosity electrodes exhibit a higher specific capacity compared to cells containing the lower porosity electrodes.

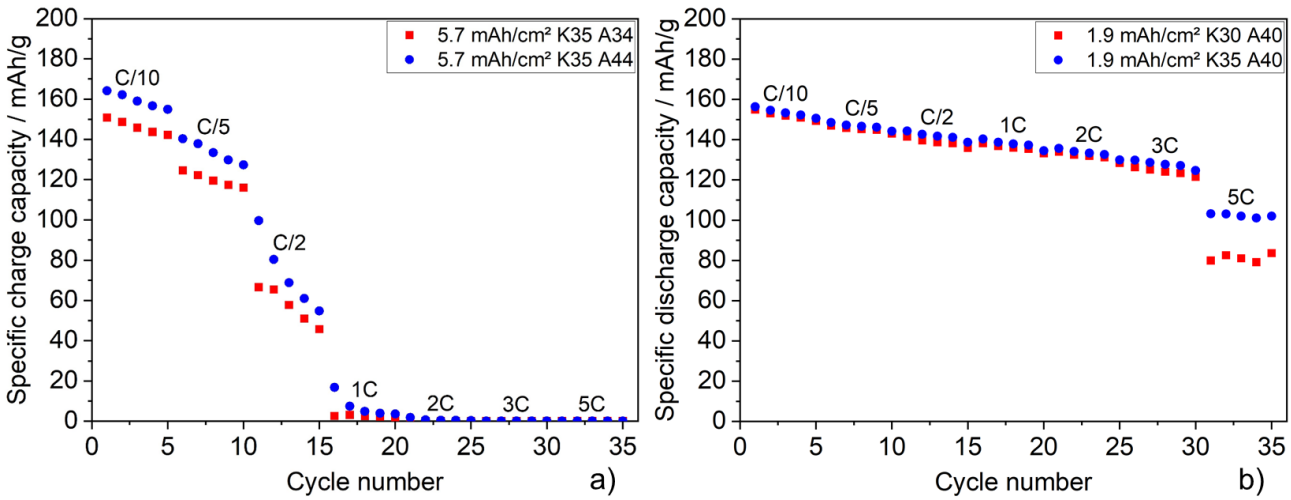

Figure 1: Rate capability analyses of a) cells containing anodes with different porosities using asymmetric charging protocol and b) cells having cathodes with different porosities using asymmetric discharging protocol.

3.3 Laser structuring

The first set of 3D electrode structures were analyzed using a scanning electron microscope (Phenom XL G2, Thermo Fischer Scientific, USA) as illustrated in Figure 2 for the cathodes and Figure 3 for the anodes. Notably, there is a significant variation in both ablation depth and width due to changes in electrode porosity: the ablation depth decreases while width increases with reducing electrode porosity.

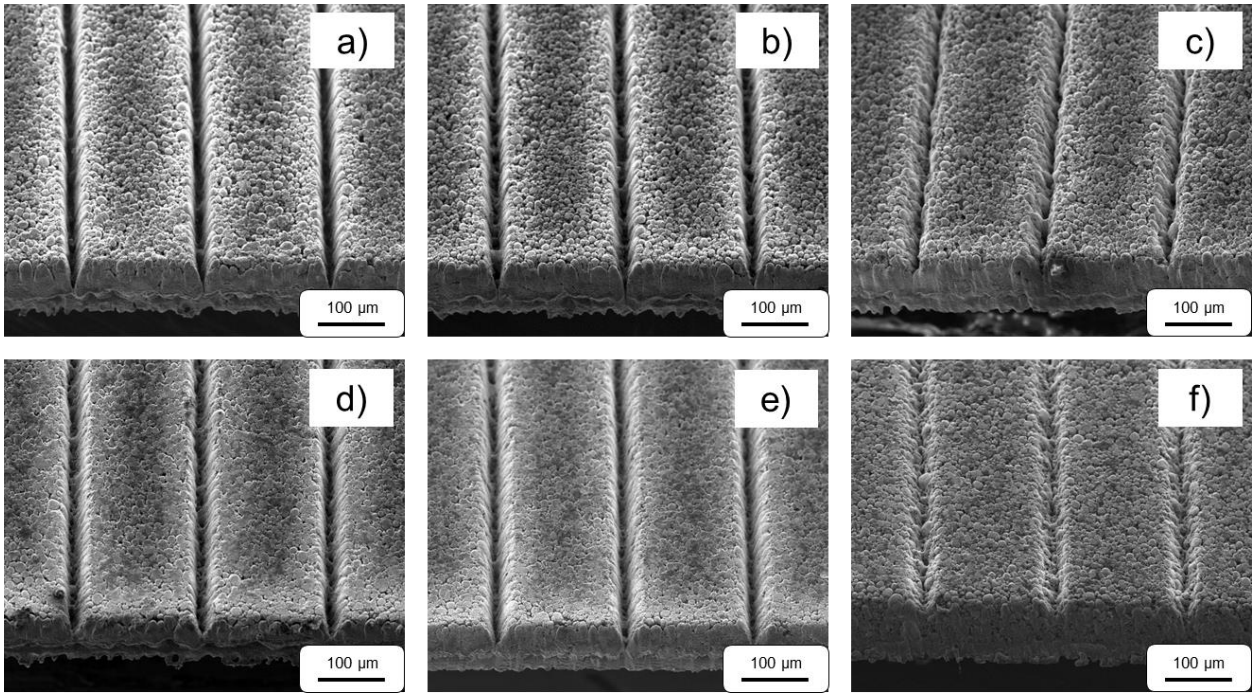

Figure 2: Scanning electron microscopy images of laser-structured NMC 622 cathodes – 35 % porosity represented by a, b, c and 24 % porosity represented by images d, e, f. Each set of images corresponds to a specific laser setup: images a and d with laser setup 1, images b and e with laser setup 2, and images c and f with laser setup 3.

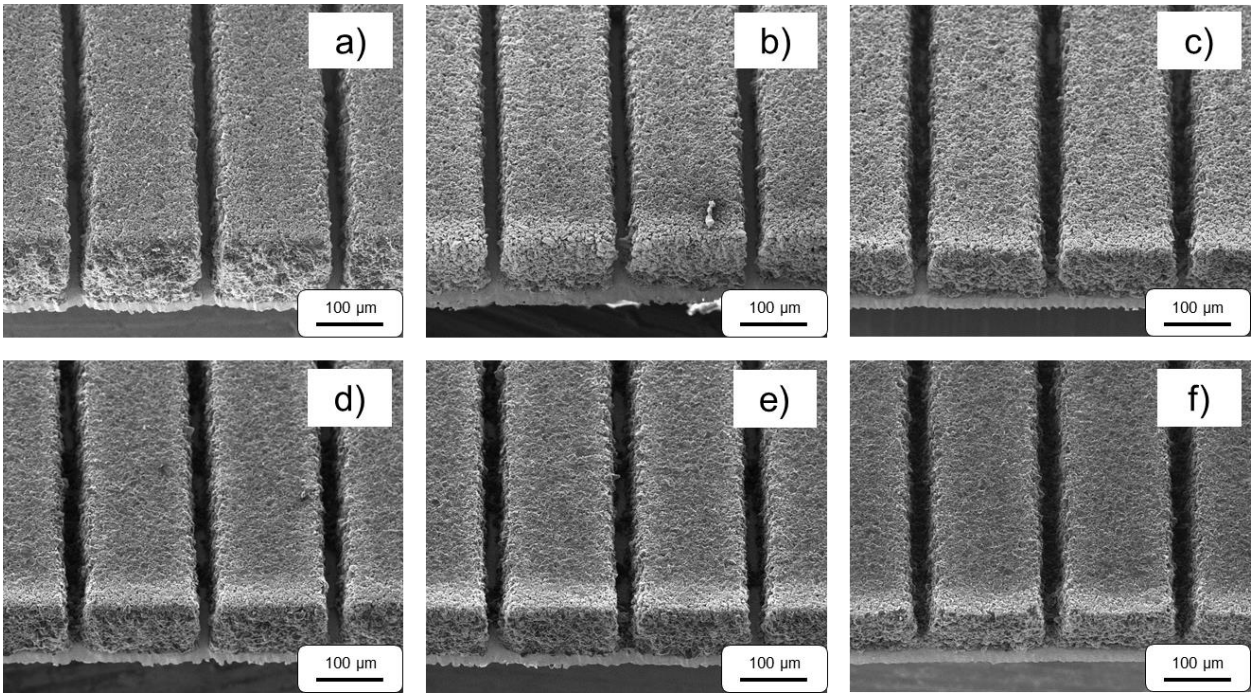

Figure 3: Scanning electron microscopy images of laser-structured graphite anodes – 45 % porosity represented by a, b, c and 35 % porosity represented by images d, e, f. Each set of images corresponds to a specific laser setup: images a and d with laser setup 1, images b and e with laser setup 2, and images c and f with laser setup 3.

The second set of 3D electrode structures were examined using an optical microscope (MeF3A, Reichert Jung, Leica Microsystems GmbH), as shown in Figure 4 for the cathodes and Figure 5 for the anodes. Similar to the first set of structures, electrode porosity has a significantly impact on the dimensions of the structured lines. A decreased ablation depth and increased ablation width were observed in electrodes with decreasing porosity.

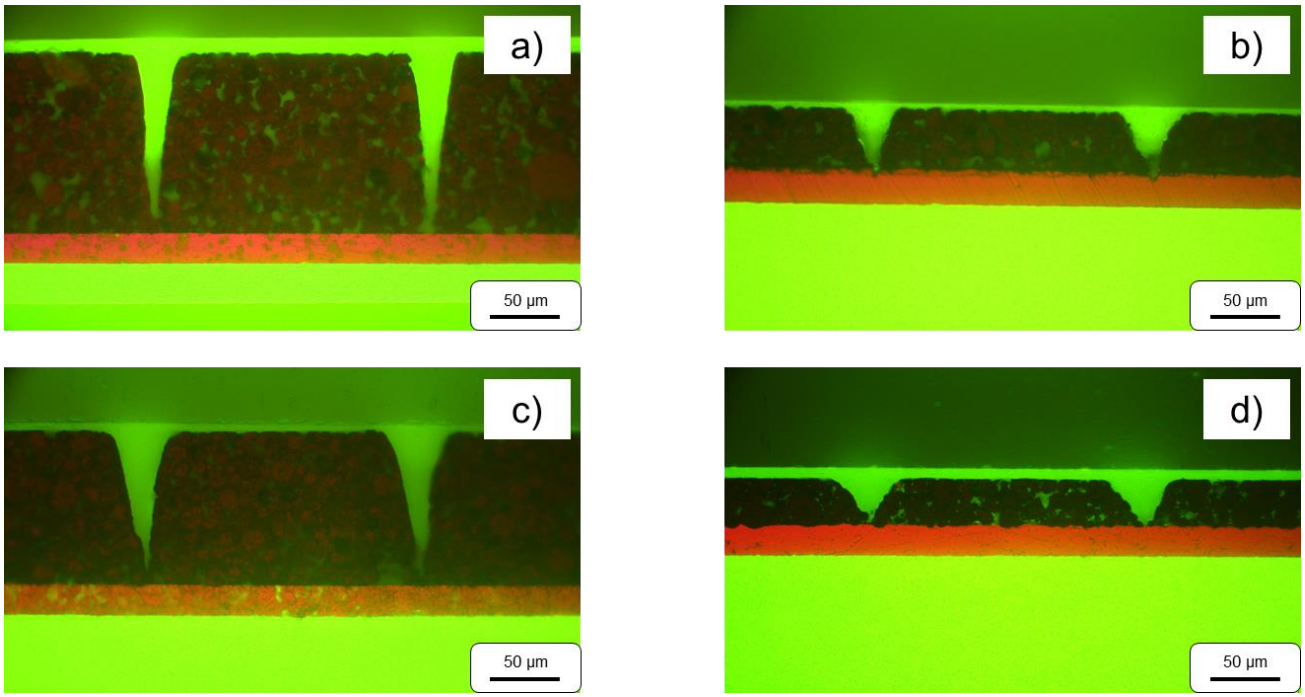

Figure 4: Cross sectional views of laser-structured NMC 622 cathodes – 35 % porosity (represented by a and b) and 22 % porosity (represented by images c and d). Each set of images corresponds to a specific electrode thickness: images a and b with a high thickness and images c and d with a low thickness. In each view laser setup 4 was used.

The previously determined reduced ablation at lower porosities is supported by the evaluation of the necessary passes for the NMC cathodes and the characterization of the structures shown in Table 7. Here it becomes clear that in comparison of Table 7a to Table 7c, 15 % more passes are necessary. This behavior can also be seen at Table 7b and Table 7d with 8 % more necessary passes.

Table 7: The number of passes and coating thickness of the groove structures in different types of NMC 622 cathodes.

Electrode type	Number of passes	Coating thickness [µm]
Thick coating with high porosity	66	129.1
Thick coating with low porosity	78	109.6
Thin coating with high porosity	22	48.0
Thin coating with low porosity	24	31.6

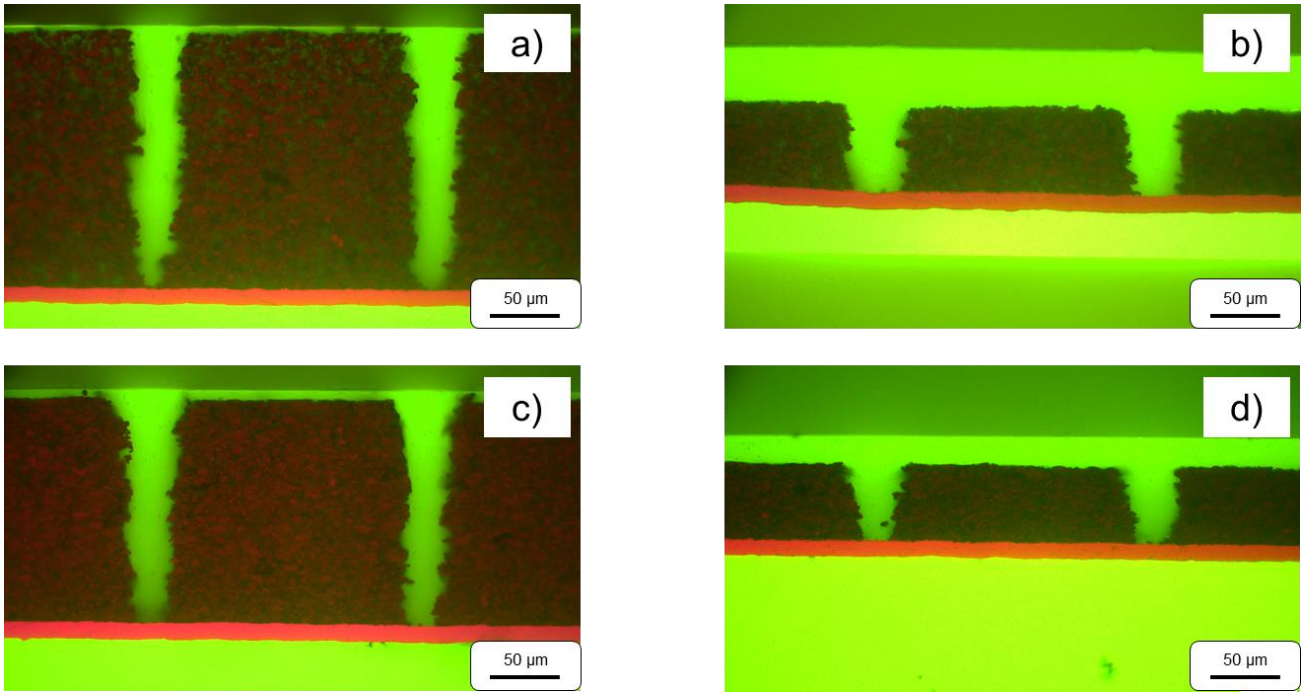

Figure 5: Cross sectional views of laser-structured graphite anodes – 45 % porosity (represented by a and b) and 35 % porosity (represented by images c and d). Each set of images corresponds to a specific electrode thickness: images a and b with a high thickness and images c and d with a low thickness. In each view laser setup 4 was used.

The results for the graphite anodes are very similar. When comparing Table 8a to Table 8c, 16 % more passes are necessary. This is also supported by the comparison of Table 8b to Table 8d with 41 % more passes.

Table 8: The number of passes and coating thickness of the groove structures in different types of graphite anodes.

Electrode type	Number of passes	Coating thickness [µm]
Thick coating with high porosity	61	186.3
Thick coating with low porosity	73	160.5
Thin coating with high porosity	10	62.6
Thin coating with low porosity	17	55.2

4. CONCLUSION

This study has demonstrated distinct correlations between the electrode porosity and the electrochemical performance as well as the ablation process for the 3D electrode structures. Our findings reveal that lower porosities lead to an increased number of passes to expose the current collector, suggesting a denser material influences the ability to effectively ablate the electrode material. Additionally, electrochemical analyses show that electrodes with lower porosities exhibit a decrease in specific capacity, affirming the critical role that porosity plays in the LIBs.

The insights gained from this study will serve as a basis for further experiments to research the correlation of the 3D electrode structures and the electrode porosity. By focusing on the interplay between these topics, we aim to refine our approach to electrode design and open up further opportunities to optimize LIBs for specific use cases, for example to achieve high volumetric energy and power density. In the next phase of our work, we will extend the study to the electrochemical investigation of structured electrodes with high and low porosity and realize these experiments in pouch cells.

ACKNOWLEDGEMENT

We are grateful to our colleagues Alexandra Reif and Heino Besser for their support during laser processing and analytics. This research has received funding from the European Union's Horizon Europe Research and innovation programme under Grant Agreement no. 101069705.

REFERENCES

[1] Bashir, T., Ismail, S.A., Song, Y., Irfan, R.M., Yang, S., Zhou, S., Zhao, J., Gao, L., 2022. A review of the energy storage aspects of chemical elements for lithium-ion based batteries. Energy Materials 1, https://doi.org/10.20517/energymater.2021.20

[2] Link, S., Neef, C., Wicke, T., 2023. Trends in Automotive Battery Cell Design: A Statistical Analysis of Empirical Data. Batteries 9, https://doi.org/10.3390/batteries9050261

[3] Shi, X., Pan, J., Wang, H., et al., 2019. Battery electric vehicles: What is the minimum range required?, Energy, https://doi.org/10.1016/j.energy.2018.10.056

[4] Ntombela, M., Musasa, K., Moloi, K., 2023. A Comprehensive Review for Battery Electric Vehicles (BEV) Drive Circuits Technology, Operations, and Challenges. World Electric Vehicle Journal 14, https://doi.org/10.3390/wevj14070195

[5] Chen, K.-H., Namkoong, M. J., Goel, V., et al., 2020. Efficient fast-charging of lithium-ion batteries enabled by laser-patterned three-dimensional graphite anode architectures, Journal of Power Sources, https://doi.org/10.1016/j.jpowsour.2020.228475

[6] Pfleging, W., 2022 - 2022. 3D electrode architectures for high energy and high power lithium-ion batteries. In: Balaya, P. et al. [Editors] Energy Harvesting and Storage: Materials, Devices, and Applications XII. SPIE. 2, https://doi.org/10.1117/12.2623655

[7] Pfleging, W., 2020. Recent progress in laser texturing of battery materials: a review of tuning electrochemical performances, related material development, and prospects for large-scale manufacturing. International Journal of Extreme Manufacturing 3, https://doi.org/10.1088/2631-7990/abca84

[8] Song, Z., Zhu, P., Pfleging, W., Sun, J., 2021. Electrochemical Performance of Thick-Film Li(Ni0.6Mn0.2Co0.2)O2 Cathode with Hierarchic Structures and Laser Ablation. Nanomaterials 11, https://doi.org/10.3390/nano11112962

[9] Jan Bernd Habedank. 2021. Laser Structuring of Graphite Anodes for Functionally Enhanced Lithium-Ion Batteries. Dissertation. München

[10] Primo, Emiliano N.; Chouchane, Mehdi; Touzin, Matthieu; Vazquez, Patricia; Franco, Alejandro A., 2021. Understanding the calendering processability of Li(Ni0.33Mn0.33Co0.33)O2-based cathodes. In: Journal of Power Sources 488, https://doi.org/10.1016/j.jpowsour.2020.229361

[11] Zheng, Honghe; Tan, Li; Liu, Gao; Song, Xiangyun; Battaglia, Vincent S., 2012. Calendering effects on the physical and electrochemical properties of Li[Ni1/3Mn1/3Co1/3]O2 cathode. In: Journal of Power Sources 208, https://doi.org/10.1016/j.jpowsour.2012.02.001.

[12] Sheng, Y., Fell, C.R., Son, Y.K., Metz, B.M., Jiang, J., Church, B.C., 2014. Effect of Calendering on Electrode Wettability in Lithium-Ion Batteries. Frontiers in Energy Research 2, https://doi.org/10.3389/fenrg.2014.00056